# Hexadirectional Modulation of Theta Power in Human Entorhinal Cortex during Spatial Navigation

## Highlights

- Intracranial EEG is acquired from epilepsy patients during spatial navigation

- Entorhinal theta power exhibits hexadirectional modulation by movement direction

- Hexadirectional modulation of theta power emerges gradually over time

- Hexadirectional modulation of theta power is sensitive to environmental boundaries

## Authors

Dong Chen, Lukas Kunz, Wenjing Wang, ..., Shuli Liang, Nikolai Axmacher, Liang Wang

## Correspondence

nikolai.axmacher@rub.de (N.A.), lwang@psych.ac.cn (L.W.)

## In Brief

Examining iEEG from epilepsy patients performing a spatial navigation task, Chen et al. find that entorhinal theta power exhibits hexadirectional modulation by movement direction, reminiscent of grid cell-like representations detected via fMRI. This hexadirectional modulation emerges gradually over time and is sensitive to environmental boundaries.

CellPress

# Hexadirectional Modulation of Theta Power in Human Entorhinal Cortex during Spatial Navigation

Dong Chen,[1,10] Lukas Kunz,[2,10] Wenjing Wang,[1] Hui Zhang,[3] Wen-Xu Wang,[1,4] Andreas Schulze-Bonhage,[2] Peter C. Reinacher,[5] Wenjing Zhou,[6] Shuli Liang,[7] Nikolai Axmacher,[3,11,*] and Liang Wang[8,9,11,12,*]

[1]School of Systems Science, Beijing Normal University, Xinjiekouwai Str. 19, 100875 Beijing, China
[2]Epilepsy Center, Medical Center—University of Freiburg, Faculty of Medicine, University of Freiburg, Breisacher Str. 64, 79106 Freiburg im Breisgau, Germany
[3]Department of Neuropsychology, Institute of Cognitive Neuroscience, Faculty of Psychology, Ruhr University Bochum, Universitätsstraße 150, 44801 Bochum, Germany
[4]State Key Laboratory of Cognitive Neuroscience and Learning & IDG/McGovern Institute for Brain Research, Beijing Normal University, Xinjiekouwai Str. 19, 100875 Beijing, China
[5]University Medical Center, Stereotactic and Functional Neurosurgery, Breisacher Str. 64, 79106 Freiburg im Breisgau, Germany
[6]Department of Epilepsy Center, Tsinghua University Yuquan Hospital, 5 Shijingshan Road, 100049 Beijing, China
[7]Department of Neurosurgery, First Affiliated Hospital of General Hospital of PLA, 51 Fucheng Road, 100048 Beijing, China
[8]CAS Key Laboratory of Mental Health, Institute of Psychology, 16 Lincui Road, 100101 Beijing, China
[9]CAS Center for Excellence in Brain Science and Intelligence Technology, 320 Yue Yang Road, 200031 Shanghai, China
[10]These authors contributed equally
[11]These authors contributed equally
[12]Lead Contact
*Correspondence: nikolai.axmacher@rub.de (N.A.), lwang@psych.ac.cn (L.W.)
https://doi.org/10.1016/j.cub.2018.08.029

## SUMMARY

Grid cells and theta oscillations are fundamental components of the brain's navigation system. Grid cells provide animals [1, 2] and humans [3, 4] with a spatial map of the environment by exhibiting multiple firing fields arranged in a regular grid of equilateral triangles. This unique firing pattern presumably constitutes the neural basis for path integration [5–8] and may also enable navigation in visual and conceptual spaces [9–12]. Theta frequency oscillations are a prominent mesoscopic network phenomenon during navigation in both rodents and humans [13, 14] and encode movement speed [15–17], distance traveled [18], and proximity to spatial boundaries [19]. Whether theta oscillations may also carry a grid-like signal remains elusive, however. Capitalizing on previous fMRI studies revealing a macroscopic proxy of sum grid cell activity in human entorhinal cortex (EC) [20–22], we examined intracranial EEG recordings from the EC of epilepsy patients (n = 9) performing a virtual navigation task. We found that the power of theta oscillations (4–8 Hz) exhibits 6-fold rotational modulation by movement direction, reminiscent of grid cell-like representations detected using fMRI. Modulation of theta power was specific to 6-fold rotational symmetry and to the EC. Hexadirectional modulation of theta power by movement direction only emerged during fast movements, stabilized over the course of the experiment, and showed

sensitivity to the environmental boundary. Our results suggest that oscillatory power in the theta frequency range carries an imprint of sum grid cell activity potentially enabled by a common grid orientation of neighboring grid cells [23].

## RESULTS AND DISCUSSION

### Behavioral Results

Epilepsy patients (n = 9) performed an object-location memory task by navigating freely in a virtual environment (Figures 1A–1E) [21]. During an initial learning phase, patients had to collect eight different objects from different locations within the environment. Afterward, patients were repeatedly asked to navigate to the location of each object. During each trial, patients were first presented with an object, navigated to the previously learned object location, received feedback, and re-encoded the object location afterward. Patients conducted the task for a period of 45 to 70 min (mean ± SD, 59.4 ± 11.9 min), which was post-hoc segmented into six non-overlapping parts ("sessions") of equal length for analysis. Patients improved throughout the experiment (repeated-measures ANOVA, $F(5,40) = 13.27$, p < 0.001; Figure 1 and STAR Methods), performing above chance level already in session 1 (one-sample t tests against chance level, all $t(8) > 3.22$, all p < 0.01). Movement directions were uniformly sampled through the entire 360° space (subject-wise Rayleigh's tests, all z < 0.01, all $P_{corr} > 0.99$, Bonferroni correction; Figure 1D) and also did not show clustering in 60° space (subject-wise Rayleigh's tests, all z < 0.92, $P_{corr} > 0.50$, Bonferroni correction; for further behavioral control analyses, Figure S1) ruling out potential confounds when analyzing a hexadirectional
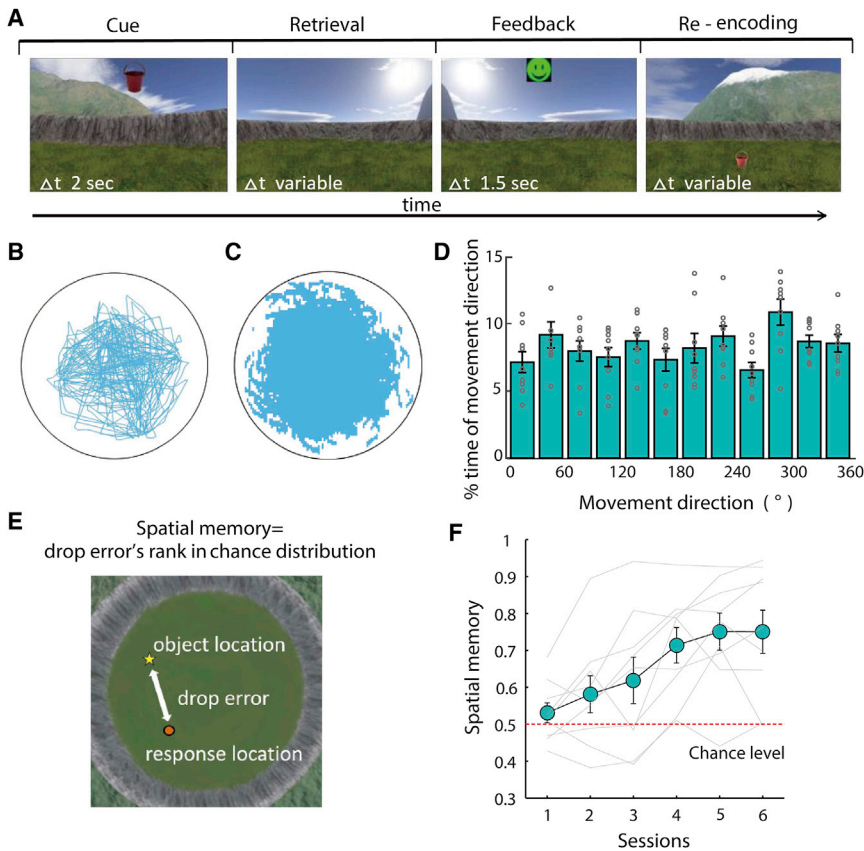
**Figure 1. Paradigm and Behavioral Results**

(A) Epilepsy patients (n = 9) implanted with iEEG electrodes in the EC performed an object-location memory task.

(B) Exemplary navigation path of one subject.

(C) Map of visited locations across all subjects.

(D) Sampling of heading direction. Gray dots show patient-wise data.

(E) Drop error defined as the distance between the response and the correct object location. Spatial memory performance was calculated as the rank of the empirical drop error within a surrogate distribution of drop errors (STAR Methods).

(F) Spatial memory performance increased throughout the experiment. Gray lines show patient-wise data.

Error bars indicate SEM across participants. See also Figure S1 and Tables S1 and S2.

modulation (HM) of intracranial electroencephalography (iEEG) power by movement direction (Figure 2A).

## Hexadirectional Modulation of Theta Power by Movement Direction in Human EC

During the task, we recorded iEEG from the entorhinal cortex (EC) (Figures 2B [25 EC electrodes in total] and S2). To uncover a potential hexadirectional (i.e., 6-fold rotationally symmetric) modulation of power from entorhinal iEEG activity, we extracted the oscillatory power in six predefined frequency bands (delta, 2–4 Hz; theta, 4–8 Hz; alpha, 8–12 Hz; beta, 12–30 Hz; low gamma, 30–80 Hz; high gamma, 80–150 Hz). We then applied the same analytical procedure as in previous fMRI studies testing for 6-fold rotationally symmetric modulation of oscillatory power by movement direction [8, 12, 20, 21] (STAR Methods): one-half of the data (sessions 1, 3, and 5) served to identify a "preferred" movement direction φ related to strongest increases of iEEG power in 60° space separately for each frequency band and for each electrode channel. In the second half of the data (sessions 2, 4, and 6), we then tested whether oscillatory power in each band was higher during movements aligned to this preferred direction as compared to misaligned movements (using a continuous cosine regressor). The resulting β coefficient of the cosine regressor quantifies the HM of iEEG power by movement direction. As in previous studies [20, 21], we only considered the fastest tertile of movement periods. We observed 6-fold rotationally symmetric modulation of power in the theta frequency band ($t(8) = 4.23$, $P_{corr} = 0.02$, Bonferroni correction for six frequency bands; Figure 2C). When

collapsing across all channels from all patients, we found that 20 of the 25 EC channels showed positive β values (fixed-effects binomial test, p = 0.004). No other frequency band showed this effect (all other $t(8) < 2.63$, $P_{corr} > 0.18$, Bonferroni correction). A one-way repeated-measures ANOVA with "frequency band" as independent variable supported the specificity of 6-fold rotationally symmetric modulation of power in the theta frequency band ($F(5,40) = 4.00$, p = 0.005). Theta power was modulated across the entire 360° range (Figures 2D and S2G). Estimated preferred directions were not clustered across participants (Rayleigh's test, z = 0.13, p = 0.88; Figure S2F) and were not related to the most sampled movement direction (Figures S2D and S2E), and no HM of iEEG power was detected during movements at slow or medium speed (Figure S2B), in line with previous fMRI results [20]. When performing the analysis of HM of iEEG power based on patient-specific theta frequency peaks (Figure S3A) determined via MODAL ([24, 25]; Figure 2E), the result of hexadirectional modulation of theta power (HM_{theta-power}) by movement direction was qualitatively identical ($t(8) = 3.97$, p = 0.004). The strength of HM based on patient-specific theta frequency peaks was positively correlated with the strength of HM based on the *a priori* defined theta band (Pearson's r = 0.83, p = 0.006; Figure 2F). Additionally, the preferred directions obtained via patient-specific theta frequency peaks were highly similar to the preferred directions obtained via the *a priori* defined theta band (circular-to-circular correlation, r = 0.89, p = 0.0001; Figure 2G).

## Specificity of HM_{theta-power} by Movement Direction in Human EC

Next, we performed control analyses to examine the specificity of our finding regarding different rotational symmetries and different brain regions. We did not find a modulation of theta power by movement direction with 4-, 5-, 7-, or 8-fold rotational symmetry (all $t(8) < 1.24$, $P_{corr} > 0.96$, Bonferroni correction; Figure 3A). Furthermore, no HM_{theta-power} was observed in
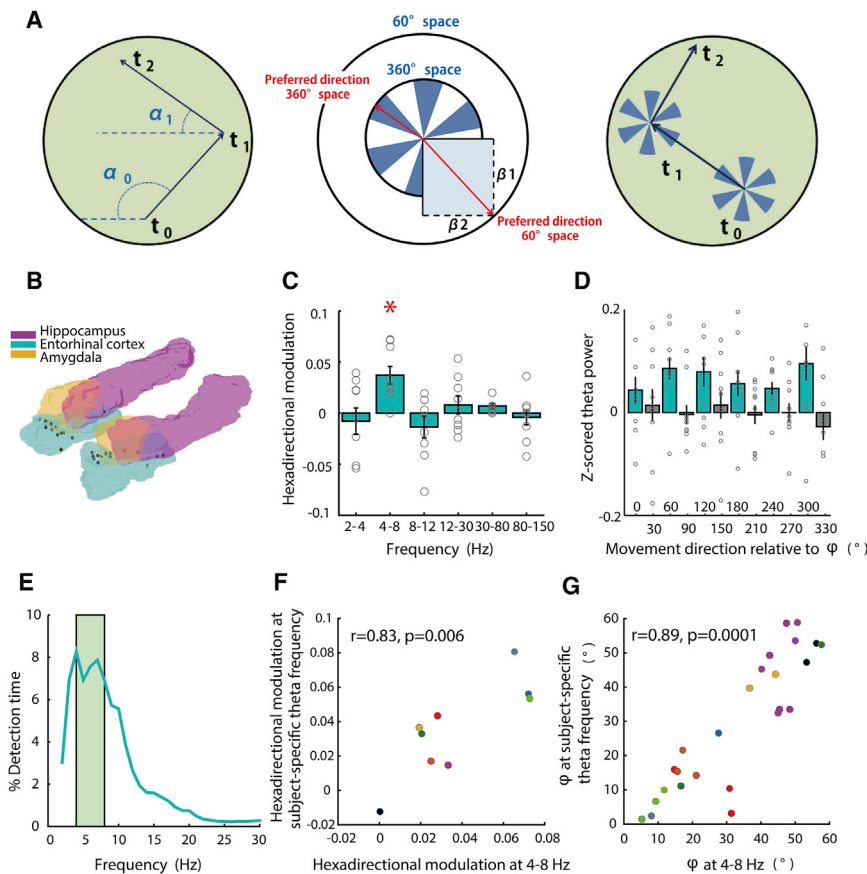
**Figure 2. Entorhinal Theta Power Exhibits 6-fold Rotationally Symmetric Modulation by Movement Direction**

(A) Analysis procedure. (Left and Middle) Using one data half, we estimated the "preferred" movement direction related to strongest increases of iEEG power in 60° space. (Right) The other data half was used to test whether oscillatory power was higher during movements aligned with the grid axes as compared to misaligned movements (STAR Methods). $\alpha$, movement direction; $t$, time point. Blue wedges, aligned; transparent wedges, misaligned.

(B) Depiction of all EC electrode contacts (black circles).

(C) 6-fold rotationally symmetric modulation of oscillatory power by movement direction in the theta frequency range, but not at any other frequency band.

(D) Theta power is higher during movements aligned with the grid axes as compared to misaligned movements. Blue, aligned; gray, misaligned.

(E) Percentage of time during which MODAL [24] detected a given instantaneous oscillatory frequency across patients.

(F) Analyzing HM based on patient-specific theta frequency peaks (Figure S3A) revealed similar results.

(G) Preferred directions obtained when analyzing HM based on patient-specific theta frequency peaks were similar to the preferred directions when performing the analysis based on the *a priori* defined theta band.

All bar plots indicate mean and SEM across participants. See also Figures S2 and S3.

hippocampus (64 channels in 8 patients; $t(7) = 0.74$, p = 0.48; 31 of the 64 channels showed positive $\beta$ values; fixed-effects binomial test, p = 0.901) or in amygdala (24 channels in 7 patients; $t(6) = 0.41$, p = 0.69; Figure 3B; 14 of the 24 electrode channels showing positive $\beta$ values; fixed-effects binomial test, p = 0.541), consistent with a reduced amount of grid cells [3] and absent grid cell-like representations in fMRI [21] in these regions. Power in different frequency bands did not depend on movement speed (3 speed levels × 6 frequency bands repeated-measures ANOVA; no interaction, $F(10,80) = 1.08$, p = 0.39; Figure S2C).

## Gradual Emergence of HM_theta-power

Since grid cells stabilize across time [1], we tested for a gradual emergence of the HM_theta-power across the experiment (employing only the fastest tertile of movement periods). On the one hand, we used the data from sessions 1 and 2 to estimate the preferred directions and tested these preferred directions on sessions 3 and 4. On the other hand, we used the data from sessions 3 and 4 to estimate the preferred directions and tested these preferred directions on sessions 5 and 6. We observed HM_theta-power by movement direction when employing sessions 3 to 6 ($t(8) = 2.64$, p = 0.03), but not when analyzing sessions 1 to 4 ($t(8) = -.15$, p = 0.89). The difference is significant ($t(8) = 2.57$, p = 0.03; Figure 3C), indicating that the HM_theta-power by movement direction became stronger over the course of the experiment. This result may parallel findings in rodents showing that grid cells stabilize across time [1] and may suggest that grid

cell-like representations in fMRI are gradually established after exposure to a novel environment.

## Sensitivity of HM_theta-power to Environmental Boundaries

Finally, we tested whether the strength of HM_theta-power depended on the movement area within the circular virtual environment. Since grid cells are stabilized by encounters with environmental boundaries in rodents [26], one may hypothesize that the HM_theta-power is particularly pronounced in more peripheral parts of the virtual environment. To this end, we divided the movement trajectory into a border, a middle, and an inner navigation region (separately for each patient; Figure S3B) containing equal numbers of fast movement periods. Indeed, we found significant HM_theta-power by movement direction when estimating the preferred direction on movements within the border area and testing the preferred direction on the middle area of the environment ($t(8) = 3.47$, p = 0.01). In contrast, we did not find a 6-fold rotationally symmetric modulation of theta power by movement direction when estimating the preferred direction on movements within the middle area and testing the preferred direction on the inner area of the environment ($t(8) = 0.80$, p = 0.45). The difference was significant ($t(8) = 2.73$, p = 0.03; Figure 3D), suggesting that the HM_theta-power by movement direction is sensitive to environmental boundaries.

In sum, the present study provides evidence for a hexadirectional modulation of theta power by movement direction in human EC during spatial navigation, reminiscent of grid
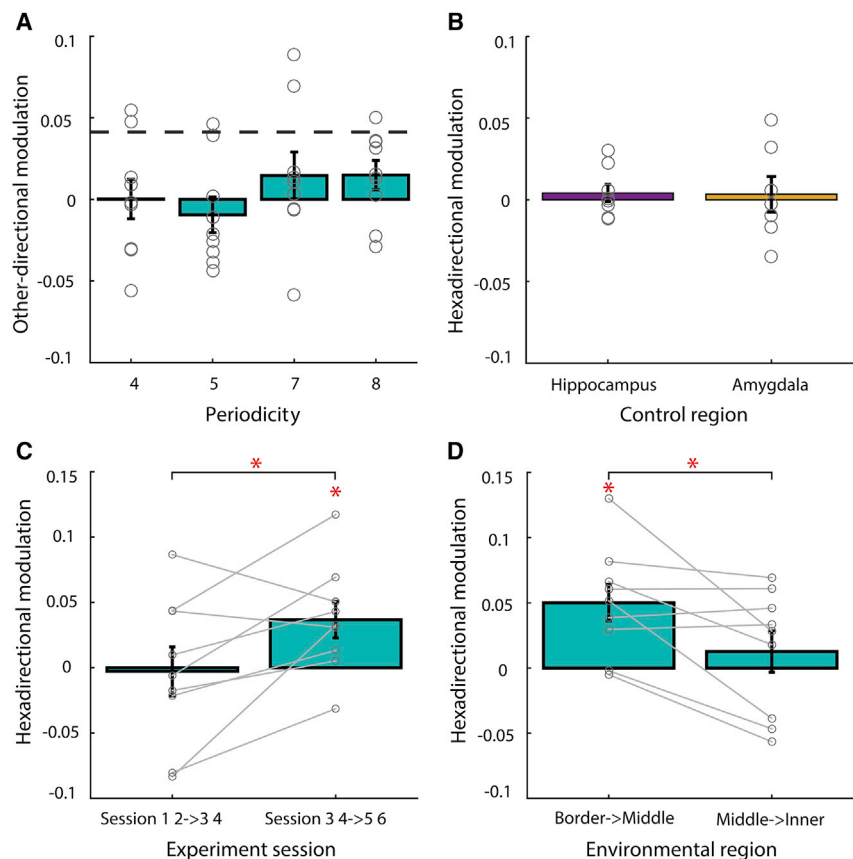
(A) Control analyses did not reveal 4-fold, 5-fold, 7-fold, or 8-fold rotationally symmetric modulation of entorhinal theta power by movement direction. Dotted line, strength of $HM_{theta-power}$ from Figure 2C.
(B) Control analyses did not reveal $HM_{theta-power}$ in hippocampus or amygdala.
(C) Entorhinal $HM_{theta-power}$ was present when examining later parts of the experiment, but not during earlier parts of the experiment.
(D) $HM_{theta-power}$ was only present during movement in peripheral parts of the virtual environment (STAR Methods). All bar plots indicate mean and SEM across participants. *$p < 0.05$.
See also Figure S3.

are scarce. Previous studies showed, in general, that independent theta generators may exist in EC and hippocampus [35] and, in the context of memory, that later remembered versus forgotten items exhibit higher entorhinal-hippocampal theta coherence during word-list learning [36]. In our study, we recorded theta oscillations from human EC during virtual navigation, revealing that theta power is hexadirectionally modulated by movement direction.

Multiple interactions between grid cells and medial temporal theta oscillations have been revealed in rodent studies. For example, grid cells in different EC layers exhibit either phase locking or phase precession in relation to entorhinal theta oscillations [37]. Grid cell properties differ depending on the phase of concurrent theta oscillations [38], and grid cells lose their periodicity after inactivation of the medial septum [39]. While theoretical models hypothesize that the firing pattern of grid cells results from interference between multiple theta generators [40], recordings in bats have demonstrated grid cells in the absence of theta oscillations [2]. The current study does not exclude either possibility but rather suggests an $HM_{theta-power}$ that may result from shared properties of neighboring grid cells.

In early studies, it was pointed out that grid cells provide an environmental-invariant metric for navigation [1]. However, recent rodent studies revealed that grid cell firing is influenced by boundaries that may distort their firing patterns [41, 42]. We used a highly regular circular environment, suggesting that firing patterns of presumably active grid cells were not substantially distorted. Our finding of higher peripheral versus central $HM_{theta-power}$ may thus be more related to evidence showing that grid stability is achieved by encounters with boundaries [26], putatively correcting for error accumulation during path integration.

Apart from grid cells, the hippocampal formation contains several other cell types structuring space and time, including place cells that encode a single location within the spatial environment [43]. Furthermore, head direction and border cells are essential components of the brain's navigation system [44, 45]. But not only spatial dimensions may be represented by the

cell-like representations observed via fMRI. Our results reveal that this $HM_{theta-power}$ emerges across time and is sensitive to environmental boundaries. From a systems perspective, our results demonstrate that neural representations occur at the level of mesoscopic oscillatory networks not only in rodents [27, 28], but also in humans [29], and suggest shared properties between single-cell responses and network activity patterns.

Since grid cells are organized in modules [23] and since conjunctive grid cells [30] increase their firing during movements aligned with the grid axes, it has been hypothesized that sum grid cell activity may be observable via fMRI [20]. Our current study suggests that a fingerprint of grid cells is also contained in mesoscopic brain oscillations. Notably, the exact relationship between grid cells and $HM_{theta-power}$ remains elusive: depending on whether grid cell activity is related to increased or decreased theta power (or increased versus decreased blood-oxygen-level dependent [BOLD] signal), movement directions denoted as "aligned" may correspond to either traverses through more grid cell firing fields (or firing fields with higher firing frequencies) or fewer firing fields (or firing fields with lower firing frequencies). This may be particularly the case, since hippocampal theta oscillations have been speculated to reflect neural firing in a similar way as alpha oscillations in the cortex [31], with higher theta power reflecting increased phasic inhibition [32].

Previous iEEG studies on spatial navigation in humans have mainly recorded theta oscillations from the hippocampus [13, 33, 34]. In contrast, studies on entorhinal theta oscillations

hippocampal formation: time cells fire at successive moments in temporally structured experiences [46]. Whether time cells exist in humans and whether they are not only detectable on single-neuron level, but also on a network level, will need to be addressed in future studies.

## STAR★METHODS

Detailed methods are provided in the online version of this paper and include the following:

- KEY RESOURCES TABLE
- CONTACT FOR REAGENT AND RESOURCES SHARING
- EXPERIMENTAL MODEL AND SUBJECT DETAILS
- METHOD DETAILS
  - Navigation task
  - Behavioral analysis
  - Intracranial EEG recordings and artifact removal
  - Electrode localization
  - Epochs of interest
  - Time-frequency analysis
  - Analysis of hexadirectional modulation of theta power by movement direction
  - Control analyses of hexadirectional modulation of theta power
  - Analysis of the emergence of hexadirectional modulation of theta power
  - Analysis of sensitivity of hexadirectional modulation of theta power to environmental boundaries
- QUANTIFICATION AND STATISTICAL ANALYSIS

### AUTHOR CONTRIBUTIONS

D.C., L.K., H.Z., A.S.-B., N.A., and L.W. designed the study. D.C., L.K., W.W., W.-X.W., W.Z., and S.L. collected data. P.C.R. implanted electrodes in Freiburg. D.C. and L.K. performed analyses. D.C., L.K., H.Z., N.A., and L.W. wrote the manuscript.

### REFERENCES

1. Hafting, T., Fyhn, M., Molden, S., Moser, M.-B., and Moser, E.I. (2005). Microstructure of a spatial map in the entorhinal cortex. Nature 436, 801–806.

2. Yartsev, M.M., Witter, M.P., and Ulanovsky, N. (2011). Grid cells without theta oscillations in the entorhinal cortex of bats. Nature 479, 103–107.

3. Jacobs, J., Weidemann, C.T., Miller, J.F., Solway, A., Burke, J.F., Wei, X.-X., Suthana, N., Sperling, M.R., Sharan, A.D., Fried, I., and Kahana, M.J. (2013). Direct recordings of grid-like neuronal activity in human spatial navigation. Nat. Neurosci. 16, 1188–1190.

4. Nadasdy, Z., Nguyen, T.P., Török, Á., Shen, J.Y., Briggs, D.E., Modur, P.N., and Buchanan, R.J. (2017). Context-dependent spatially periodic activity in the human entorhinal cortex. Proc. Natl. Acad. Sci. USA 114, E3516–E3525.

5. McNaughton, B.L., Battaglia, F.P., Jensen, O., Moser, E.I., and Moser, M.-B. (2006). Path integration and the neural basis of the 'cognitive map'. Nat. Rev. Neurosci. 7, 663–678.

6. Gil, M., Ancau, M., Schlesiger, M.I., Neitz, A., Allen, K., De Marco, R.J., and Monyer, H. (2018). Impaired path integration in mice with disrupted grid cell firing. Nat. Neurosci. 21, 81–91.

7. Banino, A., Barry, C., Uria, B., Blundell, C., Lillicrap, T., Mirowski, P., Pritzel, A., Chadwick, M.J., Degris, T., Modayil, J., et al. (2018). Vector-based navigation using grid-like representations in artificial agents. Nature 557, 429–433.

8. Stangl, M., Achtzehn, J., Huber, K., Dietrich, C., Tempelmann, C., and Wolbers, T. (2018). Compromised Grid-Cell-like Representations in Old Age as a Key Mechanism to Explain Age-Related Navigational Deficits. Curr. Biol. 28, 1108–1115.

9. Killian, N.J., Jutras, M.J., and Buffalo, E.A. (2012). A map of visual space in the primate entorhinal cortex. Nature 491, 761–764.

10. Julian, J.B., Keinath, A.T., Frazzetta, G., and Epstein, R.A. (2018). Human entorhinal cortex represents visual space using a boundary-anchored grid. Nat. Neurosci. 21, 191–194.

11. Nau, M., Navarro Schröder, T., Bellmund, J.L.S., and Doeller, C.F. (2018). Hexadirectional coding of visual space in human entorhinal cortex. Nat. Neurosci. 21, 188–190.

12. Constantinescu, A.O., O'Reilly, J.X., and Behrens, T.E.J. (2016). Organizing conceptual knowledge in humans with a gridlike code. Science 352, 1464–1468.

13. Kahana, M.J., Sekuler, R., Caplan, J.B., Kirschen, M., and Madsen, J.R. (1999). Human theta oscillations exhibit task dependence during virtual maze navigation. Nature 399, 781–784.

14. Buzsáki, G. (2002). Theta oscillations in the hippocampus. Neuron 33, 325–340.

15. Watrous, A.J., Fried, I., and Ekstrom, A.D. (2011). Behavioral correlates of human hippocampal delta and theta oscillations during navigation. J. Neurophysiol. 105, 1747–1755.

16. Hinman, J.R., Penley, S.C., Long, L.L., Escabí, M.A., and Chrobak, J.J. (2011). Septotemporal variation in dynamics of theta: speed and habituation. J. Neurophysiol. 105, 2675–2686.

17. Aghajan, M., Z Schuette, P., Fields, T.A., Tran, M.E., Siddiqui, S.M., Hasulak, N.R., Tcheng, T.K., Eliashiv, D., Mankin, E.A., Stern, J., et al. (2017). Theta Oscillations in the Human Medial Temporal Lobe during Real-World Ambulatory Movement. Curr. Biol. 27, 3743–3751.

18. Bush, D., Bisby, J.A., Bird, C.M., Gollwitzer, S., Rodionov, R., Diehl, B., McEvoy, A.W., Walker, M.C., and Burgess, N. (2017). Human hippocampal theta power indicates movement onset and distance travelled. Proc. Natl. Acad. Sci. USA *114*, 12297–12302.

19. Lee, S.A., Miller, J.F., Watrous, A.J., Sperling, M.R., Sharan, A., Worrell, G.A., Berry, B.M., Aronson, J.P., Davis, K.A., Gross, R.E., et al. (2018). Electrophysiological Signatures of Spatial Boundaries in the Human Subiculum. J. Neurosci. *38*, 3265–3272.

20. Doeller, C.F., Barry, C., and Burgess, N. (2010). Evidence for grid cells in a human memory network. Nature *463*, 657–661.

21. Kunz, L., Schröder, T.N., Lee, H., Montag, C., Lachmann, B., Sariyska, R., Reuter, M., Stirnberg, R., Stöcker, T., Messing-Floeter, P.C., et al. (2015). Reduced grid-cell-like representations in adults at genetic risk for Alzheimer's disease. Science *350*, 430–433.

22. Horner, A.J., Bisby, J.A., Zotow, E., Bush, D., and Burgess, N. (2016). Grid-like Processing of Imagined Navigation. Curr. Biol. *26*, 842–847.

23. Stensola, H., Stensola, T., Solstad, T., Frøland, K., Moser, M.-B., and Moser, E.I. (2012). The entorhinal grid map is discretized. Nature *492*, 72–78.

24. Watrous, A.J., Miller, J., Qasim, S.E., Fried, I., and Jacobs, J. (2018). Phase-tuned neuronal firing encodes human contextual representations for navigational goals. eLife *7*.

25. Cohen, M.X. (2014). Fluctuations in oscillation frequency control spike timing and coordinate neural networks. J. Neurosci. *34*, 8988–8998.

26. Hardcastle, K., Ganguli, S., and Giocomo, L.M. (2015). Environmental boundaries as an error correction mechanism for grid cells. Neuron *86*, 827–839.

27. Agarwal, G., Stevenson, I.H., Berényi, A., Mizuseki, K., Buzsáki, G., and Sommer, F.T. (2014). Spatially distributed local fields in the hippocampus encode rat position. Science *344*, 626–630.

28. Wilber, A.A., Skelin, I., Wu, W., and McNaughton, B.L. (2017). Laminar Organization of Encoding and Memory Reactivation in the Parietal Cortex. Neuron *95*, 1406–1419.

29. Watrous, A.J., Fell, J., Ekstrom, A.D., and Axmacher, N. (2015). More than spikes: common oscillatory mechanisms for content specific neural representations during perception and memory. Curr. Opin. Neurobiol. *31*, 33–39.

30. Sargolini, F., Fyhn, M., Hafting, T., McNaughton, B.L., Witter, M.P., Moser, M.-B., and Moser, E.I. (2006). Conjunctive representation of position, direction, and velocity in entorhinal cortex. Science *312*, 758–762.

31. Lisman, J.E., and Jensen, O. (2013). The θ-γ neural code. Neuron *77*, 1002–1016.

32. Mehta, M.R., Lee, A.K., and Wilson, M.A. (2002). Role of experience and oscillations in transforming a rate code into a temporal code. Nature *417*, 741–746.

33. Watrous, A.J., Lee, D.J., Izadi, A., Gurkoff, G.G., Shahlaie, K., and Ekstrom, A.D. (2013). A comparative study of human and rat hippocampal low-frequency oscillations during spatial navigation. Hippocampus *23*, 656–661.

34. Bohbot, V.D., Copara, M.S., Gotman, J., and Ekstrom, A.D. (2017). Low-frequency theta oscillations in the human hippocampus during real-world and virtual navigation. Nat. Commun. *8*, 14415.

35. Mormann, F., Osterhage, H., Andrzejak, R.G., Weber, B., Fernández, G., Fell, J., Elger, C.E., and Lehnertz, K. (2008). Independent delta/theta rhythms in the human hippocampus and entorhinal cortex. Front. Hum. Neurosci. *2*, 3.

36. Fell, J., Klaver, P., Elfadil, H., Schaller, C., Elger, C.E., and Fernández, G. (2003). Rhinal-hippocampal theta coherence during declarative memory formation: interaction with gamma synchronization? Eur. J. Neurosci. *17*, 1082–1088.

37. Hafting, T., Fyhn, M., Bonnevie, T., Moser, M.-B., and Moser, E.I. (2008). Hippocampus-independent phase precession in entorhinal grid cells. Nature *453*, 1248–1252.

38. Newman, E.L., Climer, J.R., and Hasselmo, M.E. (2014). Grid cell spatial tuning reduced following systemic muscarinic receptor blockade. Hippocampus *24*, 643–655.

39. Brandon, M.P., Bogaard, A.R., Libby, C.P., Connerney, M.A., Gupta, K., and Hasselmo, M.E. (2011). Reduction of theta rhythm dissociates grid cell spatial periodicity from directional tuning. Science *332*, 595–599.

40. Burgess, N., Barry, C., and O'Keefe, J. (2007). An oscillatory interference model of grid cell firing. Hippocampus *17*, 801–812.

41. Stensola, T., Stensola, H., Moser, M.-B., and Moser, E.I. (2015). Shearing-induced asymmetry in entorhinal grid cells. Nature *518*, 207–212.

42. Krupic, J., Bauza, M., Burton, S., Barry, C., and O'Keefe, J. (2015). Grid cell symmetry is shaped by environmental geometry. Nature *518*, 232–235.

43. O'Keefe, J., and Dostrovsky, J. (1971). The hippocampus as a spatial map. Preliminary evidence from unit activity in the freely-moving rat. Brain Res. *34*, 171–175.

44. Taube, J.S., Muller, R.U., and Ranck, J.B., Jr. (1990). Head-direction cells recorded from the postsubiculum in freely moving rats. I. Description and quantitative analysis. J. Neurosci. *10*, 420–435.

45. Solstad, T., Boccara, C.N., Kropff, E., Moser, M.-B., and Moser, E.I. (2008). Representation of geometric borders in the entorhinal cortex. Science *322*, 1865–1868.

46. MacDonald, C.J., Lepage, K.Q., Eden, U.T., and Eichenbaum, H. (2011). Hippocampal "time cells" bridge the gap in memory for discontiguous events. Neuron *71*, 737–749.

47. Gelinas, J.N., Khodagholy, D., Thesen, T., Devinsky, O., and Buzsáki, G. (2016). Interictal epileptiform discharges induce hippocampal-cortical coupling in temporal lobe epilepsy. Nat. Med. *22*, 641–648.

48. Jenkinson, M., Beckmann, C.F., Behrens, T.E.J., Woolrich, M.W., and Smith, S.M. (2012). FSL. Neuroimage *62*, 782–790.

49. Qin, C., Tan, Z., Pan, Y., Li, Y., Wang, L., Ren, L., Zhou, W., and Wang, L. (2017). Automatic and Precise Localization and Cortical Labeling of Subdural and Depth Intracranial Electrodes. Front. Neuroinform. *11*, 10.

## STAR★METHODS

### KEY RESOURCES TABLE

| REAGENT or RESOURCE | SOURCE | IDENTIFIER |
|---|---|---|
| Software and Algorithms | | |
| MATLAB 2017b | The MathWorks, Natick, MA, USA | https://www.mathworks.com/products/new_products/release2017b.html |
| IBM SPSS Statistics for Windows, Version 24.0 | Armonk, NY: IBM | https://www.ibm.com/products/spss-statistics |
| Freesurfer v6.0.0 | Athinoula A. Martinos Center for Biomedical Imaging at Massachusetts General Hospital | surfer.nmr.mgh.harvard.edu/ |
| FSL | FMRIB, Oxford, UK | https://fsl.fmrib.ox.ac.uk/fsl/fslwiki/FSL |
| PyLocator | Thorsten Kranz | http://pylocator.thorstenkranz.de/ |

### CONTACT FOR REAGENT AND RESOURCES SHARING

Further information and requests for resources and reagents should be directed to and will be fulfilled by the Lead Contact, Liang Wang (lwang@psych.ac.cn).

### EXPERIMENTAL MODEL AND SUBJECT DETAILS

Intracranial EEG was recorded from medically intractable epilepsy patients who underwent stereotactic (non-robotic) electrode implantation for localizing their epileptic seizure foci to guide respective treatment. Electrode placement was determined solely by clinical needs. N = 11 patients participated in this study. Two patients were excluded from all analyses due to intense epileptic activity within the EC. This left 9 patients (3 female, 7 right handed) with a mean age ± STD of 27.1 ± 8.2 years (see Table S1 for further details). Our research protocol was approved by the appropriate institutional review boards at the different recording sites. Written informed consent was obtained from all patients.

### METHOD DETAILS

#### Navigation task
Participants performed an object-location memory task navigating freely in a circular virtual arena adapted from Doeller et al. [20]. The environment comprised a grassy plane (diameter of 9,500 virtual units) bounded by a cylindrical cliff. The navigation task was programmed using Unreal Engine 2 (Epic Games). During an initial learning phase at the beginning of the experiment, patients were asked to navigate toward and memorize the locations of 8 different everyday objects. Afterward, patients completed variable numbers of trials. Each trial consisted of a cue, a retrieval, a feedback, and a re-encoding phase (Figure 1A). During the cue phase, participants were presented with one of the objects (duration = 2 s). During the retrieval phase, they navigated to the associated object location using the arrow keys on the laptop keyboard (left, right, and forward arrows). The duration of this phase was self-paced. When they had reached the location they considered correct, they "dropped" the object by hitting the space bar or the backward arrow key. Depending on response accuracy, patients then received feedback via one of five possible smiley faces (duration = 1.5 s). The object then appeared at its correct location, and patients navigated to this location, allowing for further learning. Participants controlled their movement speed by modulating the duration how long they pressed the forward button. Continuously pressing the forward button automatically accelerated movement speed until maximum speed was reached. The task was run on a laptop with a screen at approximately 30 cm distance from the patient. Behavioral events including the subject's location within the virtual environment were written to a logfile with a temporal resolution of 10 ms. Triggers were either detected using a phototransistor attached to the screen marking onsets and offsets of the cue-phase, or using an independent custom MATLAB (2017b, The MathWorks, Massachusetts) program that sent triggers both to the paradigm as well as to the EEG recording software with randomly jittered intervals between 0.5 s and 5 s. Patients were asked to complete up to 160 trials, but were instructed to pause or quit the task whenever they wanted.

#### Behavioral analysis
For each time point, we extracted the participant's location in the virtual environment, which enabled us to derive movement direction and movement speed. For each patient, we checked whether movement directions were uniformly sampled both through the entire $360°$ space and through $60°$ space employing subject-wise Rayleigh's tests ruling out the possibility that our finding of

hexadirectional modulation of theta power was due to non-uniform sampling of movement directions. Further behavioral control analyses were performed for movements within the three different environmental regions, specifically for fast movements (Figures S1 and S2). Spatial memory performance was estimated by ranking the trial-wise drop error (distance between drop location and correct location; Figure 1E) with respect to a surrogate distribution obtained by calculating the distance between 500,000 randomly chosen locations within the virtual environment and the correct location. A spatial memory score of 1 represents a perfect response, whereas a score of 0 represents a response at maximal distance from the correct location. A score of 0.5 represents chance level. To test whether patients improved gradually throughout the experiment, we calculated a one-way repeated-measures ANOVA with "session number" as independent variable and "spatial memory performance" as dependent variable. Additionally, we performed one-sample t tests of spatial memory performance values against 0.5 (i.e., chance-level), separately for each session, to test whether patients performed above chance-level in each session.

### Intracranial EEG recordings and artifact removal

Intracranial EEG recordings were performed at the Yuquan Hospital, Tsinghua University, Beijing, China; at the First Affiliated Hospital of PLA General Hospital, Beijing, China; and at the Department of Epileptology, University of Freiburg, Freiburg, Germany. Our research protocol was approved by the appropriate institutional review boards at each of the three hospital sites. Written informed consent was obtained from all patients. During recordings, all patients had normal or corrected-to-normal vision. At the recording sites in Beijing, iEEG data was acquired using a Nihon-Kohden system (Yuquan Hospital) and a Blackrock Neuroport system (First Affiliated Hospital of PLA General Hospital) at a sampling rate of 2,000 Hz. At the recording site in Freiburg iEEG data was acquired using a Compumedics system (Compumedics, Abbotsford, Victoria, Australia) at a sampling rate of 2,000 Hz. Electrodes were provided by HKHS Beijing Health (HKHS Beijing Health, Beijing, China) at Yuquan Hospital and First Affiliated Hospital of PLA General Hospital, or Ad-Tech (Ad-Tech, Racine, WI, USA) at the Department of Epileptology, University of Freiburg. Recordings were referenced to Cz (Freiburg) or to one electrode contact located in white matter (Beijing). Regarding the latter, candidate reference electrode contacts located in white matter were chosen by visual inspection of the post-implantation CT images co-registered onto the pre-implantation MR images (see below). Then, intracranial EEG traces from each candidate reference electrode were visually inspected, and contacts with little or no apparent EEG activity were chosen as the reference for all subsequent recordings (see reference 18 for a similar procedure). Electrode contacts from three different regions of interest were analyzed: EC (9 subjects; 25 contacts; range of contacts per subject, 1-8), hippocampus (8 subjects; 64 contacts; range of contacts per subject, 0-16), and amygdala (7 subjects; 24 contacts; range of contacts per subject, 0-7; see Table S1 for further details).

No seizure was observed 1 h before or after the tests in all patients. Recordings, which included all experimental sessions performed by each patient as well as several minutes of EEG from before and after those sessions, were first inspected for interictal spikes (IIS) and other artifacts by an automatic removal procedure. Epileptic discharges were identified and excluded when one of the following two criteria were met: (i) the envelope of the unfiltered signal was 4 standard deviations above the baseline (i.e., the mean value of the entire signal); (ii) the envelope of the filtered signal (band-pass filtered in the 25-80 Hz range followed by signal rectification) was 5 standard deviations above the baseline (i.e., the mean value of the filtered signal) following previous studies [17, 47]. All iEEG traces were also visually inspected for epileptic activity, both before and after the automatic removal procedure. The timing of all IISs and other artifacts on each channel were stored for subsequent analysis.

### Electrode localization

For patients from Freiburg, for whom one pre-implantation and one post-implantation MRI were available, electrode localization was performed using FSL (https://fsl.fmrib.ox.ac.uk/fsl/fslwiki/FSL) [48] and PyLocator (http://pylocator.thorstenkranz.de/): The post-implantation MR image was coregistered to the pre-implantation MR image. Next, the pre-implantation MR image was skull-stripped and normalized to MNI space, applying the normalization matrix to the post-implantation MR image in parallel. Normalized post-implantation images were inspected using PyLocator and channel locations were manually identified. For patients from Beijing, post-implantation CT images were co-registered onto pre-implantation MR images using Freesurfer (v6.0.0, surfer.nmr.mgh.harvard.edu/). The registration was visually verified and manually adjusted if necessary. Intracranial electrodes were identified using clustering-based segmentation and classified according to anatomical landmarks in native space [49]. For visualization of all subjects' electrodes on the average brain surface, each individual subject's MRI was coregistered to the MNI space. All electrodes were then superimposed onto the inflated brain. Location of electrode contacts was ascertained by visual inspection of post implantation CT and/or MRI scans by a consultant neurophysiologist and MRI expert.

### Epochs of interest

Analysis of iEEG recordings focused on fast movement epochs following [20, 21]. As in previous studies [20, 21], fast movement epochs were defined as the fastest tertile of all movements which are separately determined for each participant (Table S2). For control analyses regarding movement speed, epochs of interest were also extracted for medium speed movements (movements with a speed between the fastest and slowest tertile) and slow speed movements (slowest tertile of movements). For additional control analyses, stationary periods during which patients did not move were also extracted.

### Time-frequency analysis

First, the raw data of the entire experiment was notch-filtered at 50 Hz as well as at harmonics of 50 Hz. Next, all epochs that included interictal spikes or other artifacts were excluded from further analyses. Afterward, the entire data were band-pass filtered in 6 different frequency bands (delta, 2-4Hz; theta, 4-8Hz; alpha, 8-12Hz; beta, 12-30Hz; low gamma, 30-80Hz; and high gamma, 80-150Hz). We first converted the data into the frequency domain using the *fft* function in MATLAB, then applied a Gaussian function with a STD of 0.7 Hz for attenuation at the respective border frequencies, and converted the data back into the time domain using the *ifft* function in MATLAB. Subsequently, oscillatory power of each band at each electrode channel was extracted using a Hilbert transform. The power values were then z-scored according to the mean power in that electrode over all fast movement epochs (defined as movements above the cut-off speed, see Table S2). For control analyses regarding movement speed, power values were z-scored according to the mean power in that electrode over all medium or slow movement epochs, respectively. To test whether band power varied as a function of frequency band and movement speed, we calculated a two-way (3 speed levels x 6 frequency bands) repeated-measures ANOVA.

### Analysis of hexadirectional modulation of theta power by movement direction

To reveal a potential hexadirectional modulation of theta power by movement direction, we closely followed the procedure of estimating grid cell-like representations in prior fMRI studies. The initial learning phase was excluded from all analyses. First, we aligned the iEEG time courses with the sampling rate of the behavioral data (100 Hz), and averaged power values of each frequency band within consecutive non-overlapping 10 ms time windows. After extracting periods of fast movements, movement directions ($\alpha_t$) over time were split into 6 sessions according to the total experiment duration of each participant (irrespective of trial phase and trial number). Using one half of the data (sessions 1, 3, and 5), we identified the "preferred" movement direction $\varphi$ related to strongest increases of iEEG power in each frequency band. To do so, we modeled the band power using a general linear model (GLM) with two regressors, $\cos(6\alpha_t)$ and $\sin(6\alpha_t)$. This resulted in two weights of the two regressors, $\beta_{cos}$ and $\beta_{sin}$, which were then used to calculate the preferred direction $\phi = [\arctan(\beta_{sin}/\beta_{cos})]/6$ using the *atan2* function in MATLAB. The overall duration of the data segment used to perform this GLM was 133.9 ± 46.9 s (mean ± STD; fast speed), 127.1 ± 39.1 s (medium speed), and 123.2 ± 41.7 s (slow speed). Using the second half of the data (sessions 2, 4, and 6), we then used a second GLM with a single predictor $\cos(6(\alpha_t - \phi))$ to examine whether band power increased when the patient moved closer to the preferred direction $\phi$. The second GLM gave the weight $\beta_{aligned}$ quantifying the six-fold rotationally symmetric modulation of theta power by movement direction, which was termed "grid cell-like representations" in previous fMRI studies [20]. The higher $\beta_{aligned}$ the higher the band power when the patient is moving closer to the preferred direction $\phi$. The factor 6 accounts for six-fold rotational symmetry. The overall duration of the data segment used to perform this GLM was 139.1 ± 52.3 s (mean ± STD; fast speed), 128.1 ± 40.4 s (medium speed), and 115.7 ± 34.8 s (slow speed). If a patient was implanted with more than one electrode channel in her/his entorhinal cortex, $\beta_{aligned}$-values were averaged across electrode channels. Afterward, (averaged) $\beta_{aligned}$-values were fed into second-level statistics across patients. One-sample t tests across patients were performed to test whether hexadirectional modulation of theta power was present during fast movement periods for any of the six frequency bands (including Bonferroni correction for multiple comparisons by multiplying the *P*-values by 6, since we tested for this effect in 6 different frequency bands). To illustrate that theta power was modulated by movement direction across the entire 360° range, all fast movement periods were distributed onto 12 different movement bins (each of 30° size) relative to the patient-specific preferred direction (6 aligned bins, 6 misaligned bins). Theta power was determined for each of the twelve bins and averaged across patients afterward. To reveal whether theta power increases during aligned movements were absolute or relative power increases (with regard to stationary periods), we performed a variant of this analysis during which we employed theta power values that had been normalized using the mean and standard deviation of theta power during stationary periods. To test whether preferred directions estimated using the first half of the data clustered at a specific angle across patients, we performed a Rayleigh test. If a patient was implanted with more than one electrode channel in her/his entorhinal cortex, the circular mean of the channel-wise preferred directions was fed into the Rayleigh test.

### Control analyses of hexadirectional modulation of theta power

We performed several control analyses to validate the presence of hexadirectional modulation of theta power with regard to fast movement speed, 6-fold rotational symmetry, and entorhinal cortex. Regarding movement speed, we performed the identical analysis procedure as outlined above on time periods of medium and slow movement speed, respectively. One-sample t tests were performed across patients to examine whether theta power exhibited six-fold rotationally symmetric modulation by movement direction during medium or slow speed movements. Furthermore, we checked whether theta power during fast speed movements was modulated by movement direction with regard to other types of rotational symmetry (i.e., 4-, 5-, 7-, and 8-fold rotational symmetry). Again, the identical analysis procedure as outlined above was performed, now using the factors 4, 5, 7, or 8, respectively, when setting up the regressors for the first and the second GLM (e.g., $\cos(4\alpha_t)$ and $\sin(4\alpha_t)$ for the first GLM, and $\cos(4(\alpha t - \phi))$ for the second GLM). Second-level t tests were performed across patients afterward. As a last control analysis, we applied the analysis of hexadirectional modulation of iEEG power by movement direction for electrode channels located in hippocampus and amygdala. Again, whenever a patient was implanted with more than one electrode channel in his/her hippocampus or amygdala, respectively, $\beta_{aligned}$-values were averaged across electrode channels before performing second-level statistics.

### Analysis of the emergence of hexadirectional modulation of theta power

To test for a gradual emergence of hexadirectional modulation of theta power across the experiment, we applied the analysis of hexadirectional modulation of theta power to shorter data segments. On the one hand, we used sessions 1 and 2 to estimate the preferred direction and tested this preferred direction using data from sessions 3 and 4. The resulting $\beta_{aligned}$-values represent the strength of hexadirectional modulation of theta power during the first two thirds of the experiment. On the other hand, we used sessions 3 and 4 to estimate the preferred direction and tested this preferred direction using data from sessions 5 and 6. The resulting $\beta_{aligned}$-values represent the strength of hexadirectional modulation of theta power during the last two thirds of the experiment. $\beta_{aligned}$-values were entered into second-level one-sample t tests across patients. A paired t test was used to test for a significant difference between the strength of hexadirectional modulation of theta power obtained from the two data parts.

### Analysis of sensitivity of hexadirectional modulation of theta power to environmental boundaries

To test for a sensitivity of hexadirectional modulation of theta power to environmental boundaries, we performed the analysis of hexadirectional modulation of theta power on data parts during which the patients moved within specific regions of the virtual environment. To this end, we divided all movement time points into three parts depending on whether the patient moved within the inner, the middle, or the border region of the environment. The separation of the virtual environment into the three regions was done individually such that, for each patient, each region contained $n/3$ fast movement time points, where $n$ denotes the total number of fast movement time points. On the one hand, we used fast movements within the border region to estimate the preferred direction and tested this preferred direction on data during fast movements within the middle region of the virtual environment. The resulting $\beta_{aligned}$-values represent the strength of hexadirectional modulation of theta power when moving in more peripheral parts of the virtual environment. On the other hand, we used fast movements within the middle region to estimate the preferred direction and tested this preferred direction on data during fast movements within the inner region of the environment. The resulting $\beta_{aligned}$-values represent the strength of hexadirectional modulation of theta power when moving in more central parts of the environment. $\beta_{aligned}$-values were entered into second-level one-sample t tests against 0 across patients. A paired t test was then used to test for a significant difference between the strength of hexadirectional modulation of theta power obtained from the two different analyses.

### QUANTIFICATION AND STATISTICAL ANALYSIS

All analyses were performed in MATLAB 2017b using custom MATLAB scripts. Inference statistics across patients were performed using MATLAB or SPSS (version 24.0, IBM, NY). Types of statistical tests used are specified where the test statistics are reported. If not otherwise specified, all statistical tests were performed with the final sample of 9 epilepsy patients (see above). If not otherwise specified, all statistical tests were two-sided. If not otherwise specified, means were used as definition of center and SEM were used as dispersion measure. Statistical analyses were performed using a significance threshold of $p < 0.05$. If appropriate, Bonferroni correction was applied by multiplying the output $P$-value of the test statistic by the number of tests performed. Error bars in figures are defined in the corresponding figure legends. Further details on statistical analyses are given in the Results and Discussion section and in the STAR Methods section.